Buffer layer between a planar optical concentrator and a solar cell

Manuel E. Solano, Greg D. Barber, Akhlesh Lakhtakia, Muhammad Faryad, Peter B. Monk and Thomas E. Mallouk

***Abstract*—The effect of inserting a buffer layer between a periodically multilayered isotropic dielectric (PMLID) material acting as a planar optical concentrator and a photovoltaic solar cell was theoretically investigated. The substitution of the photovoltaic material by a cheaper dielectric material in a large area of the structure could reduce the fabrication costs without significantly reducing the efficiency of the solar cell. Both crystalline silicon and gallium arsenide were considered as the photovoltaic material. We found that the buffer layer can act as an antireflection coating at the interface of the PMLID and the photovoltaic materials, and increasing the spectrally averaged electron-hole pair density by $\sim 25\%$. Relative to a solar-cell module without the POC and the buffer layer, there is an efficiency loss of 40% for c-Si solar cells and 14% for GaAs solar cells accompanied by the combination of the optimal POC and the optimal buffer layer.**

***Index Terms*—planar optical concentrator, thin-film solar cell, surface multiplasmonics**

I. Introduction

Several authors have proposed to use a laminar dielectric structure called a planar optical concentrator (POC) to steer vertically incident solar light into a horizontal path towards photovoltaic solar cells mounted on the edges [1]–[3]. The substitution of the photovoltaic material by a cheaper dielectric material in a large area of the light-harvesting structure could reduce the fabrication costs without significantly reducing the efficiency of conversion of photonic energy into electrical energy. The large-area fabrication of such composite structures using patterning techniques such as soft lithography and particle assembly [4]–[6] is now inexpensive enough that the concentrators and the photovoltaic components can have sub-mm dimensions. These micro-cell designs are forgiving with respect to the incorporation of optically lossy materials such as metals into the POC. They are also advantageous for heat dissipation, especially at the modest concentration ratios that are appropriate with relatively low-cost single-junction crystalline silicon (c-Si) and thin-film compound-semiconductor photovoltaic solar cells.

A POC comprising a periodic multilayered isotropic dielectric (PMLID) material backed by a metallic surface-relief grating was proposed and optimized earlier for crystalline-silicon (c-Si) solar cells [2]. The geometrical parameters and the refractive indexes of the materials in the POC were selected in order to maximize the solar-spectrum-integrated power-flux density inside the PMLID material. Consequently, the spectrally averaged electron-hole pair (EHP) density generated in the solar cells was also maximized. Since there is a mismatch between the optical permittivities of the PMLID constituents and the solar cell, reflection occurs at the PMLID/c-Si interfaces. If this reflection could be reduced, the conversion of photonic energy to electrical energy would be further enhanced.

Therefore, we decided to investigate the effect of an isotropic dielectric buffer layer inserted between the PMLID material and the solar cell in an effort to maximize the transfer of optical energy from the PMLID material to the solar cell. Based upon the optical permittivities of the layers in PMLID material and of the semiconductor, this buffer layer should act as an antireflection coating.

Figure 1 presents the schematic of one unit cell of the light-harvesting structure in the xz plane, the structure being invariant along the y axis. At the bottom is a metal grating of period L along the x axis. Atop one period of the metal grating sits a solar cell, atop N_c consecutive periods of the grating sits a PMLID material with N_d periods in the vertical direction, and one period each on both sides of the solar cell are shared by the PMLID material and the buffer layer. The topmost layer is indium-tin oxide (ITO) functioning as an optically transparent electrode. Using data on an optimized PMLID material [2], our objective here is to optimize the thickness L_b and the refractive index n_b of the buffer layer, when the solar cell is made of either c-Si or gallium arsenide (GaAs).

The plan of this paper is as follows. Section II provides a brief description of the theory used to compute the specular and non-specular reflectances and transmittances of the light-harvesting structure shown in Fig. 1, when it is illuminated by a linearly polarized plane wave whose propagation vector lies wholly in the xz plane. An $\exp(-i\omega t)$ dependence on time t is implicit, with ω as the angular frequency and $i =$

M. E. Solano is with the Departamento de Ingeniería Matemática and CI^{2}MA, Universidad de Concepción, Concepción, Chile and acknowledges partial financial support from CONICYT-Chile via grant FONDECYT-11130350 and BASAL project CMM, Universidad de Chile. E-mail: msolano@ing-mat.udec.cl

G. D. Barber is with the Department of Chemistry, Pennsylvania State University, University Park, PA 16802.

A. Lakhtakia is with the Department of Engineering Science and Mechanics, Pennsylvania State University, University Park, PA 16802.

M. Faryad was with the Department of Engineering Science and Mechanics, Pennsylvania State University, University Park, PA 16802. He is now with the Department of Physics, Lahore University of Management Sciences, Lahore 54792, Pakistan.

P. B. Monk is with the Department of Mathematical Sciences, University of Delaware, Newark, DE 19716.

T. E. Mallouk is with the Department of Chemistry, Pennsylvania State University, University Park, PA 16802.

M. Faryad, G. D. Barber, A. Lakhtakia, P. B. Monk and T. E. Mallouk acknowledge partial financial support from US National Science Foundation via grant DMR-1125590.

Manuscript received XX, 2014; revised XX, 2014.

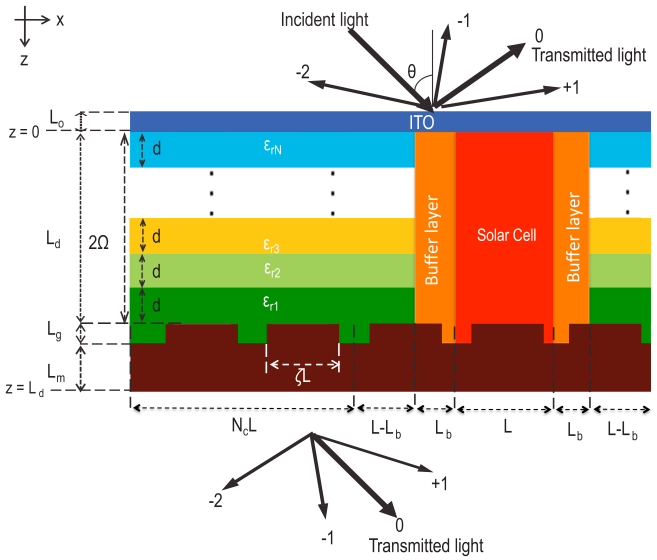

Fig. 1. Schematic of one period (along the x axis) of the light-harvesting structure. When a plane wave is incident at an angle θ with respect to the z axis, the reflected and the transmitted fields comprise specular components (labeled 0) and nonspecular components (labeled $\pm1, \pm2, ...$). A buffer layer is inserted between the PMLID material and the solar cell. The PMLID material is shown to have only one period along the z axis (i.e., $N_d = 1$).

$\sqrt{-1}$. The spectrally averaged EHP density is calculated using the computed solution. Section III presents numerical results, when the solar cell is made of either c-Si or GaAs. The paper concludes with a few remarks in Sec. IV.

II. Theory in brief

A. Geometry

Figure 1 shows the unit cell of the concentrator $\{x \in (0, N_cL + 3L), z \in (-L_o, L_t)\}$, where $L_t = L_d + L_g + L_m$. The region $z < -L_o$ is vacuous, while the top layer $\{x \in (0, N_cL + 3L), z \in (-L_o, 0)\}$ is made of indium-tin oxide.

The PMLID material occupies the regions $\{x \in (0, N_cL + L - L_b), z \in (0, L_d)\}$ and $\{x \in (N_cL + 2L + L_b, N_cL + 3L), z \in (0, L_d)\}$. Along the z axis, this material has $N_d \geq 1$ periods. Each period is of thickness $2\Omega = L_d/N_d$ and comprises N layers of equal thicknesses $d = 2\Omega/N$. The relative permittivity $\varepsilon_{rj} > 1$ of the j-th layer, $j \in [1, N]$, is taken to be a real-valued function of the free-space wavelength $\lambda_0 = 2\pi c_0/\omega$, where c_0 is the speed of light in free space. Our interest lies in the spectral regime $\lambda_0 \in [\lambda_{0_{min}}, \lambda_{0_{max}}]$ dictated by the solar spectrum.

The regions $\{x \in (0, N_cL + L - L_b), z \in (L_d, L_t)\}$ and $\{x \in (N_cL + 2L + L_b, N_cL + 3L), z \in (L_d, L_t)\}$ are occupied by a metallic surface-relief grating with its troughs filled by a dielectric material of relative permittivity ε_{r1}. The metal/dielectric interface has a periodic rectangular profile with a period L along the x axis, corrugation height L_g, and duty cycle $\zeta \in [0, 1]$. The λ_0-dependent relative permittivity of the metal is denoted by ε_m with $\mathrm{Re}(\varepsilon_m) < 0$ and $\mathrm{Im}(\varepsilon_m) > 0$.

The regions $\{x \in (N_cL + L, N_cL + 2L), z \in (0, L_d)\}$, $\{x \in (N_cL + L, N_cL + 1.5L - 0.5\zeta L), z \in (L_d, L_d + L_g)\}$, and $\{x \in (N_cL + 1.5L + 0.5\zeta L, N_cL + 2L), z \in (L_d, L_d + L_g)\}$ are occupied by a semiconductor of λ_0-dependent relative permittivity ε_s with $\mathrm{Re}(\varepsilon_s) > 0$ and $\mathrm{Im}(\varepsilon_s) > 0$.

The regions $\{x \in (N_cL + L - L_b, N_cL + L), z \in (0, L_d)\}$, $\{x \in (N_cL + 2L, N_cL + 2L + L_b), z \in (0, L_d)\}$, $\{x \in (N_cL + 0.5L + 0.5\zeta L, N_cL + L), z \in (L_d, L_d + L_g)\}$, and $\{x \in (N_cL + 2L, N_cL + 2.5L - 0.5\zeta L), z \in (L_d, L_d + L_g)\}$ are occupied by a buffer material of relative permittivity $\varepsilon_b = n_b^2 > 1$, which is taken to be non-dissipative and non-dispersive in the spectral regime of interest.

The remainder of the unit cell is occupied by a metal of relative permittivity ε_m. The half space $z > L_t$ is vacuous.

B. Plane-wave response

Suppose that the light-harvesting structure is illuminated by an obliquely incident plane wave whose electric field phasor is given by

$$\begin{aligned}\mathbf{E}_{inc}(x, z, \lambda_0) = [a_s \hat{\mathbf{u}}_y + a_p (-\hat{\mathbf{u}}_x \cos\theta + \hat{\mathbf{u}}_z \sin\theta)] \\ \exp\{ik_0 [x \sin\theta + (z + L_o)\cos\theta]\}\,, \\ z \leq -L_o\,.\end{aligned} \tag{1}$$

Here, θ is the angle of incidence with respect to the z axis, a_s is the amplitude of the s-polarized component, a_p is the amplitude of the p-polarized component, $k_0 = \omega/c_0$ is the free-space wavenumber, and $\{\hat{\mathbf{u}}_x, \hat{\mathbf{u}}_y, \hat{\mathbf{u}}_z\}$ is the triple of Cartesian unit vectors.

As depolarization cannot occur in this problem, the electric field phasors of the reflected and the transmitted fields can be stated as [7], [8]

$$\begin{aligned}\mathbf{E}_{ref}(x, z, \lambda_0) = \sum_{n\in\mathbb{Z}} \left(a_s r_{ss}^{(n)} \hat{\mathbf{u}}_y + a_p r_{pp}^{(n)} \mathbf{p}_n^-\right) \\ \exp\left\{i\left[\kappa^{(n)} x - \alpha^{(n)}(z + L_o)\right]\right\}\,, \\ z < -L_o\,,\end{aligned} \tag{2}$$

and

$$\begin{aligned}\mathbf{E}_{tr}(x, z, \lambda_0) = \sum_{n\in\mathbb{Z}} \left(a_s t_{ss}^{(n)} \hat{\mathbf{u}}_y + a_p t_{pp}^{(n)} \mathbf{p}_n^+\right) \\ \exp\left\{i\left[\kappa^{(n)} x + \alpha^{(n)}(z - L_t)\right]\right\}\,, \\ z > L_t\,,\end{aligned} \tag{3}$$

respectively, where $\mathbb{Z} \equiv \{0, \pm1, \pm2, ...\}$,

$$\kappa^{(n)} = k_0 \sin\theta + 2\pi \frac{n}{(N_c + 3)\, L}\,, \tag{4}$$

$$\alpha^{(n)} = \begin{cases} +\sqrt{k_0^2 - (\kappa^{(n)})^2}\,, & k_0^2 \geq (\kappa^{(n)})^2 \\ +i\sqrt{(\kappa^{(n)})^2 - k_0^2}\,, & k_0^2 < (\kappa^{(n)})^2 \end{cases}\,, \tag{5}$$

and

$$\mathbf{p}_n^{\pm} = \mp \frac{\alpha^{(n)}}{k_0} \hat{\mathbf{u}}_x + \frac{\kappa^{(n)}}{k_0} \hat{\mathbf{u}}_z\,. \tag{6}$$

The λ_0-dependent reflection coefficients of order n are denoted by $r_{ss}^{(n)}$ and $r_{pp}^{(n)}$, and the corresponding transmission coefficients by $t_{ss}^{(n)}$ and $t_{pp}^{(n)}$. Thus, the reflected and the transmitted

field phasors comprise specular components identified by $n = 0$ and non-specular components identified by $n \neq 0$. Provided that L_m is sufficiently thick, the transmitted field will transport virtually no energy in the $+z$ direction.

In the region $z \in (-L_o, L_t)$, the electric and magnetic field phasors must satisfy the frequency-domain Maxwell curl equations

$$\left.\begin{aligned} \nabla \times \mathbf{E}(x,z,\lambda_0) &= i\omega\mu_0 \mathbf{H}(x,z,\lambda_0) \\ \nabla \times \mathbf{H}(x,z,\lambda_0) &= -i\omega\varepsilon_0\epsilon_r(x,z,\lambda_0)\mathbf{E}(x,z,\lambda_0) \end{aligned}\right\}, \quad (7)$$

where ε_0 is the permittivity and μ_0 is the permeability of free space. We used the finite-element method (FEM) [9], [10] to solve Eqs. (7). After decoupling the s- and p-polarization states and exploiting the independence of the field phasors from y, we reduced Eqs. (7) to two scalar Helmholtz equations, one for each of the two linear polarization states. The boundary conditions on the sides $x = 0$ and $x = N_cL + 3L$ of the unit cell have to be quasi-periodic. Standard transmission conditions hold across the top boundary $z = -L_o$ and bottom boundary $z = L_t$, whose satisfaction involves Eqs. (1)–(3).

We used a special-purpose finite-element meshing function based on the TRIANGLE library [11]. Inside each triangle of the mesh, the field phasors were approximated by cubic polynomials. The summations in the expressions of the reflected and transmitted field phasors were truncated to $n \in \{-M_t, M_t\}$.

C. Spectrally averaged EHP density

After obtaining the reflection and transmission coefficients for any $\lambda_0 \in [\lambda_{0_{min}}, \lambda_{0_{max}}]$, the electric field phasor $\mathbf{E}(x,z,\lambda_0)$ can be obtained at any location inside the unit cell, for an unpolarized incident plane wave with an electric field of magnitude $E_o = 1$ V m^{-1}.

Thereafter, the spectrally averaged EHP density can be computed as [2]

$$N_{avg} = \int_{\lambda_{0_{min}}}^{\lambda_{0_{max}}} F(\lambda_0) d\lambda_0 \,, \quad (8)$$

where

$$F(\lambda_0) = \lambda_0 \frac{S(\lambda_0)\,\mathrm{Im}[\epsilon_s(\lambda_0)]}{LL_d c_0 \hbar E_0^2 \cos\theta} \left\{ \int_{x=N_cL+L}^{N_cL+2L} \left[\int_{z=0}^{z_m(x)} |\mathbf{E}(x,z,\lambda_0)|^2 dz \right] dx \right\}, \quad (9)$$

$$z_m(x) = \begin{cases} L_d + L_g \,, & x \in (N_cL + L, \\ & \quad N_cL + 1.5L - 0.5\zeta L) \\ L_d \,, & x \in (N_cL + 1.5L - 0.5\zeta L, \\ & \quad N_cL + 1.5L + 0.5\zeta L) \\ L_d + L_g \,, & x \in (N_cL + 1.5L + 0.5\zeta L, \\ & \quad N_cL + 2L) \end{cases}, \quad (10)$$

$\hbar$ is the reduced Planck constant, $S(\lambda_0)$ is the AM1.5 solar spectrum [12], $\lambda_{0_{min}} = 400$ nm, and $\lambda_{0_{max}} = 1000$ nm.

III. Numerical results

For all calculations, we set $L_o = 100$ nm, a practical value. Also, we chose the metal to be silver and $L_m = 40$ nm. As optimization of the POC alone had previously [2] provided the relative permittivities of all $N = 9$ layers in every period of the PMLID material, we used the same here as well. The values of ϵ_m and ϵ_{rj}, $j \in [1, N]$, versus λ_0 are shown in Figs. 3 and 4, respectively. We also adopted the following parameters previously found to be optimal in the absence of the buffer layer [2]: $\theta = 7$ deg, $d = 120$ nm, $N_d = 3$, $\zeta = 0.72$, $L_g = 62$ nm, and $L = 400$ nm. We also set $N_c = 2$, based on the same optimization study. Our objective was to determine L_b and n_b that maximizes N_{avg} when the solar cell is made of c-Si or GaAs.

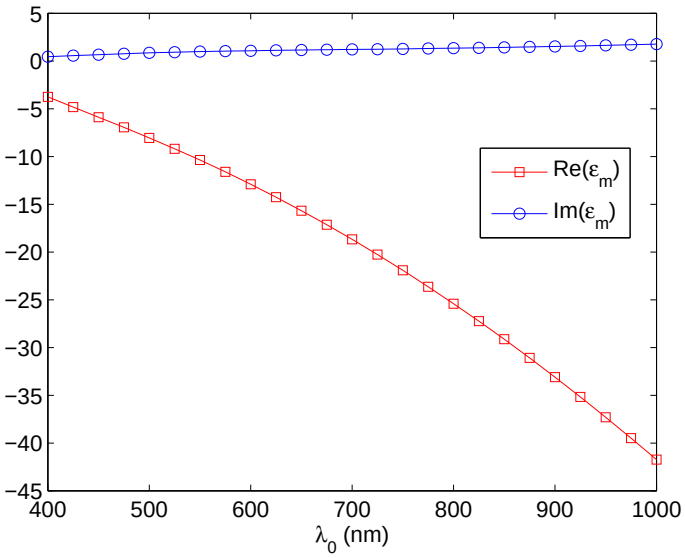

Fig. 2. Real (red squares) and imaginary (blue circles) part of relative electric permittivity ε_m of silver versus λ_0.

A. Optimization of buffer layer when $N_d = 1$

The optimal POC without the buffer layer was found by Solano *et al.* [2] to have $N_d = 3$. However, optimization of the buffer layer is going to be computationally very time consuming with $N_d = 3$, given the limitations of our computational resources. Therefore, we first optimized the buffer layer after setting $N_d = 1$ for the POC and then found the characteristics of the combination of the optimized POC with $N_d = 3$ and the optimized buffer layer. The latter results are presented in Sec. III-B.

Figure 4 shows the mesh used when $N_d = 1$. The mesh has 1792 triangles in the region $\{x \in [0, L], z \in [-L_o, L_t]\}$ (and in every other similar region of the unit cell), and each triangle is completely filled by just one dielectric material. We set $M_t = 20$ so that the truncation error for the transmitted and reflected waves would be negligible in comparison to the error inherent in partitioning space into triangles, as required by the FEM.

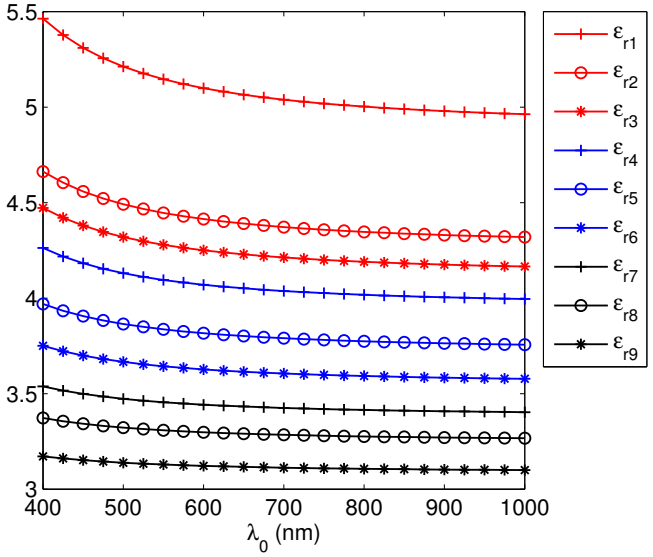

Fig. 3. Relative permittivity ε_{rj} of the j-th layer, $j \in [1, 9]$, of PMLID material versus λ_0.

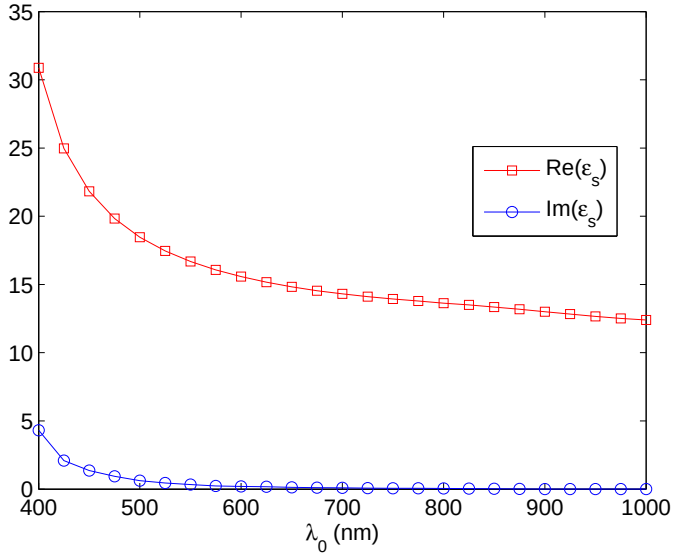

Fig. 5. Real (red squares) and imaginary (blue circles) parts of the relative permittivity ε_s of c-Si versus λ_0.

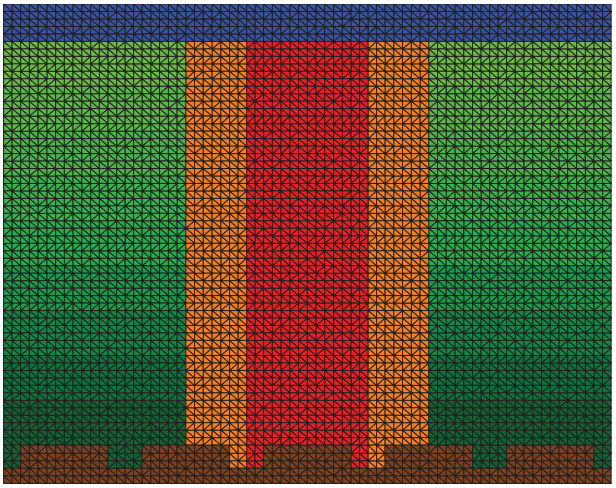

Fig. 4. FEM mesh (dark lines) of the light-harvesting structure. Colors in the background correspond to different regions: Metallic grating (brown), solar cell (red), buffer layer (orange), the PMLID material with $N_d = 1$ (green), and the ITO layer (blue).

1) c-Si solar cell: Let us first present results for the solar cell made of c-Si, whose relative permittivity is provided in Fig. 5 as a function of λ_0 [13].

In Fig. 6 the computed values of N_{avg} for $2L_b \in \{0, 58, 115, 173, 230, 288, 344, 400, 458, 515, 573, 630, 688, 744, 800\}$ nm and $n_b \in \{1.4, 1.8, 2.2, 2.6, 3.0, 3.4\}$ are displayed. The set of values of $2L_b$ was chosen so that the outer edges of the buffer layer always coincide with the mesh lines on the grid.

The spectrally averaged EHP density is always higher if a buffer layer with refractive index larger than 2.2 is present, indicating a reduction in the reflectance at the POC/solar-cell interface. In addition, for any $n_b \geq 2.2$, N_{avg} achieves a maximum at some $2L_b \in [300, 500]$ nm and decreases with further increase in $2L_b$. The data allow us to conclude that the optimal parameters of the buffer layer are: $2L_b^{opt} = 400$ nm and $n_b^{opt} = 2.6$. Then, $N_{avg}^{opt} = 1.35 \times 10^{17}$ cm^{-2} which is 23% higher than when there is no buffer layer (i.e., $2L_b = 0$).

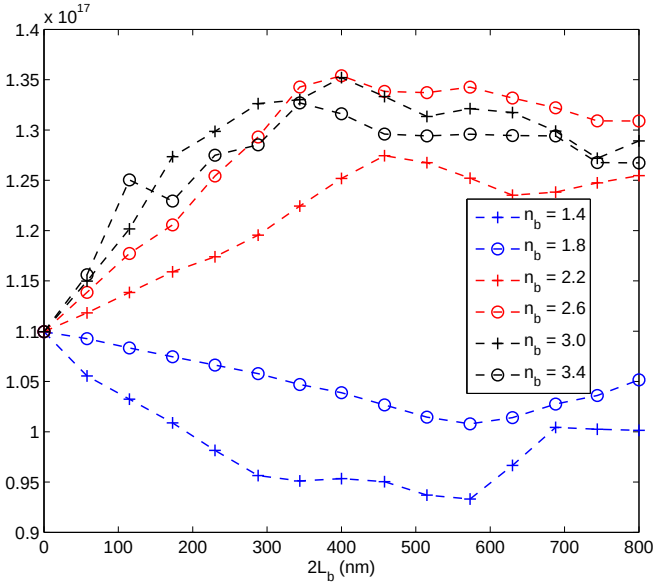

Fig. 6. N_{avg} (cm^{-2}) versus $2L_b$ for $n_b \in \{1.4, 1, 8, 2.2, 2.6, 3.0, 3.4\}$ when the solar cell is made of crystalline silicon, $N_d = 1$, and $n_b = 1.6$ (blue crosses), 1.8 (blue circles), 2.2 (red crosses), 2.6 (red circles), 3.0 (black crosses), or 3.4 (black circles).

Let us denote by F^{opt} and F^{ref} the values of F when the buffer layer is optimal (i.e., $2L_b = 400$ nm and $n_b = 2.6$) and absent (i.e., $2L_b = 0$), respectively. Figure 7 shows F^{opt} and F^{ref} as functions of λ_0. In much of the spectral regime of interest, $F^{opt} > F^{ref}$. The maximum value of the ratio F^{opt}/F^{ref} is 2.21, which occurs for $\lambda_0 = 735.44$ nm.

In Fig. 8, we present the spatial distributions of $|\mathbf{E}(x, z, \lambda_0)|^2$ in the entire structure for $2L_b \in$

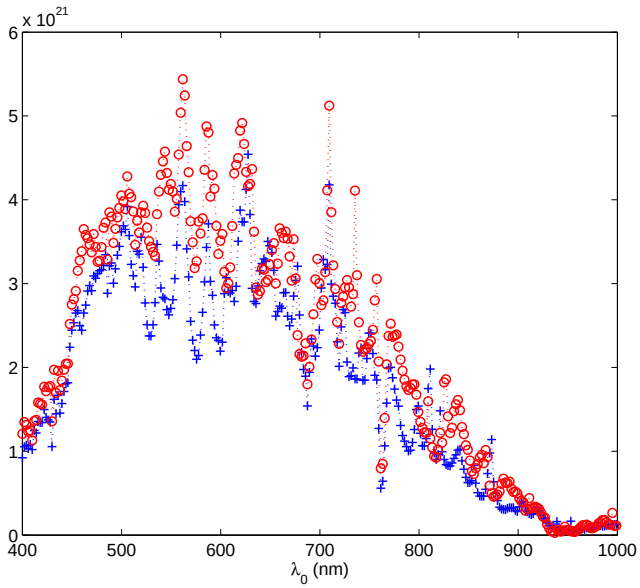

Fig. 7. F^{opt} (cm^{-3}) (red circles) and F^{ref} (cm^{-3}) (blue crosses) versus λ_0, when the solar cell is made of c-Si and $N_d = 1$.

$\{0, 230, 400, 800\}$ nm, when $\lambda_0 = 735.44$ nm, $N_d = 1$, and $n_b = 2.6$. Close to the grating, a band of hot spots occurs in the POC, the buffer layer, and the solar cell when $2L_b = 400$ nm. This band explains the doubling of F by the insertion of the optimal buffer layer. We attribute the occurrence of this band to surface-multiplasmonic effects [2], [7].

2) GaAs solar cell: We also considered the solar cell made of GaAs, whose relative permittivity is provided in Fig. 9 as a function of λ_0 [14].

Similarly to Fig. 6, the computed values of N_{avg} versus $2L_b$ and n_b are displayed in Fig. 10. These data shows that the optimal parameters are: $2L_b^{opt} = 630$ nm and $n_b^{opt} \in \{2.6, 3.0\}$. Then, $N_{avg}^{opt} = 2.92 \times 10^{17}$ cm^{-2} which is 31% higher than when there is no buffer layer (i.e., $2L_b = 0$). Moreover, in Fig. 11 we observe that across almost all wavelengths of interest, $F^{opt} > F^{ref}$. The maximum value of the ratio F^{opt}/F^{ref} is 1.82, which occurs for $\lambda_0 = 835.27$ nm.

In Fig. 12, we present the spatial distributions of $|\mathbf{E}(x, z, \lambda_0)|^2$ in the entire structure for $2L_b \in \{0, 400, 630\}$ nm, when $\lambda_0 = 835.27$ nm and $n_b = 2.6$. The intensity is higher in the solar cell when the buffer layer is present. No significant differences in intensities are observed between $2L_b = 400$ nm and $2L_b = 630$ nm.

B. Enhancement with optimal buffer layer when $N_d = 3$

The optimal buffer layers identified in Sec. III-A were combined with the optimal POC [2] for which $N_d = 3$, and the spectrally averaged EHP densities were calculated for both c-Si and GaAs solar cells.

1) c-Si solar cell: For the c-Si solar cell, the optimal values for the buffer layer were found to be $2L_b = 400$ nm and $n_b = 2.6$ in Sec. III-A1. The spectrally averaged EHP density was found to be 27% higher for $2L_b = 400$ nm than when the buffer layer is absent (i.e., $2L_b = 0$).

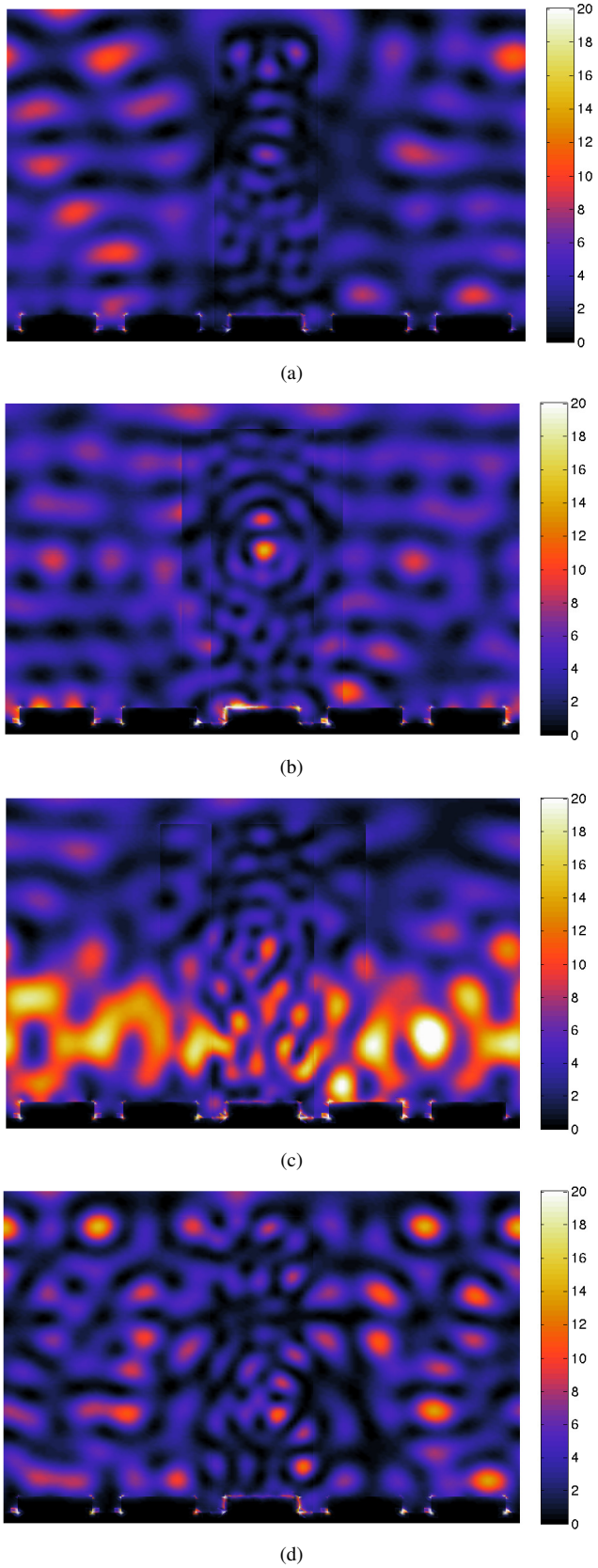

Fig. 8. Spatial distribution of $|\mathbf{E}(x, z, \lambda_0)|^2$ (V^2 m^{-2}) inside a unit cell of the light-harvesting structure the incident light is unpolarized, $\lambda_0 = 735.44$nm, the solar cell is made of c-Si, $N_d = 1$, and $n_b = 2.6$. (a) $2L_b = 0$, (b) $2L_b = 230$ nm, (c) $2L_b = 400$ nm, and (d) $2L_b = 800$ nm.

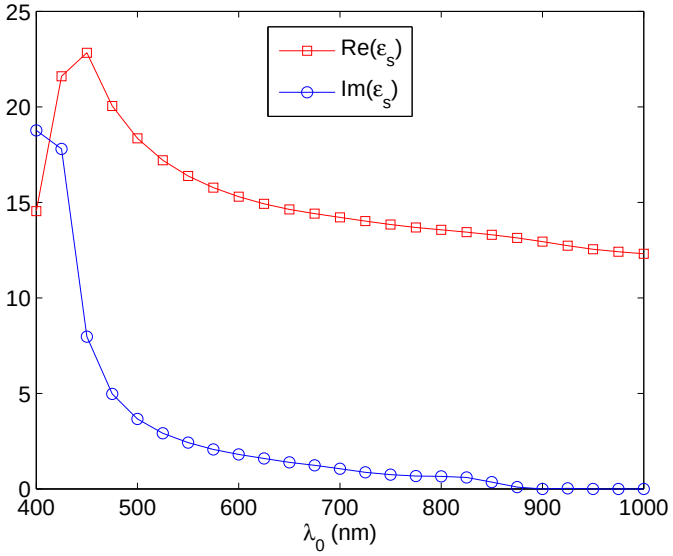

Fig. 9. Real (red squares) and imaginary (blue circles) parts of the relative permittivity ε_s of GaAs versus λ_0.

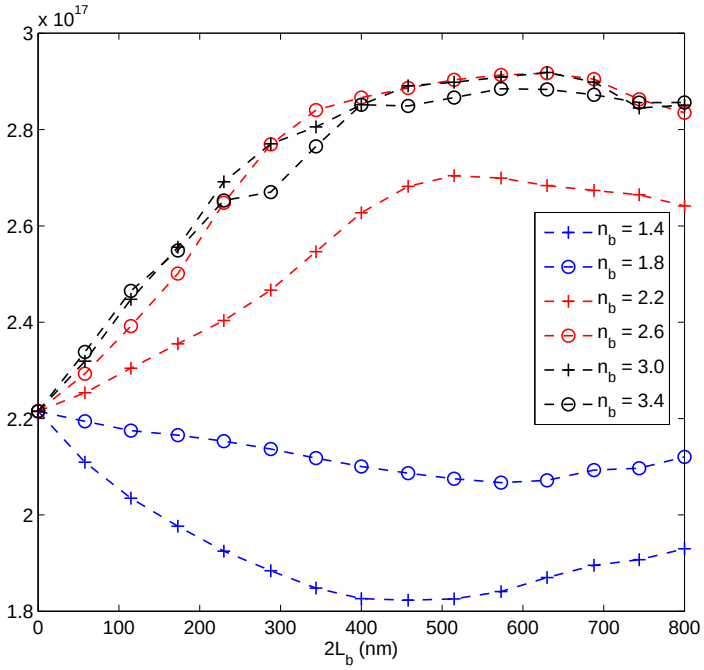

Fig. 10. N_{avg} (cm^{-2}) versus $2L_b$ for $n_b \in \{1.4, 1, 8, 2.2, 2.6, 3.0, 3.4\}$ when the solar cell is made of GaAs, $N_d = 1$, and $n_b = 1.6$ (blue crosses), 1.8 (blue circles), 2.2 (red crosses), 2.6 (red circles), 3.0 (black crosses), or 3.4 (black circles).

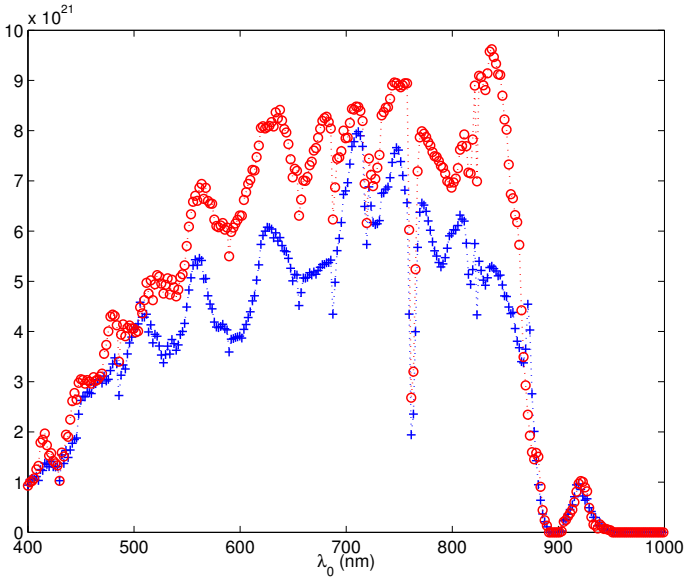

Fig. 11. F^{opt} (cm^{-3}) (red circles) and F^{ref} (cm^{-3}) (blue crosses) versus λ_0, when the solar cell is made of GaAs and $N_d = 1$.

Figure 13 shows F versus λ_0 when $2L_b = 0$ nm (blue crosses) and $2L_b = 400$ nm (blue circles). We clearly observe an enhancement of F when the buffer layer is included. The maximum value of the ratio F^{opt}/F^{ref} is 2.49, which occurs for $\lambda_0 = 919.13$ nm. Extremely high values of $|\mathbf{E}(x, z, \lambda_0)|^2$ are observed in presence of the optimal buffer layer, as is evident from a comparison of Fig. 14(a) for $L_b = 0$ with Fig. 14(b) for $2L_b = 400$ nm.

On a per-unit-area basis, replacement of 80% of the solar cell by the the optimal POC will lead to a 53.6% loss in efficiency. However, replacement of a part of the POC by the optimal buffer layer reduces the efficiency loss to 40%. The use of very cheap dielectric materials for the POC and the buffer layer could offset this reduction.

2) GaAs solar cell: Finally we present our results for the GaAs solar cell, considering $N_d = 3$ and the optimal values $2L_b = 630$ nm and $n_b = 2.6$ obtained from subsection III-A2. We found that N_{avg} increases by 41% when the optimal buffer layer is introduced.

The plots of F^{opt} (for $2L_b = 630$ nm) and F^{ref} (for $L_b = 0$ nm) with respect to λ_0 in Fig. 15 indicate that $F^{opt} > F^{ref}$ for most of the spectral regime of interest, with the largest value of F^{opt}/F^{ref} being 2.21 at $\lambda_0 = 945.09$ nm. Fig. 16 shows $|\mathbf{E}(x, z, \lambda_0)|^2$ for $2L_b \in \{0, 630\}$ nm, when $\lambda_0 = 945.09$ nm and $n_b = 2.6$. We again observe very high intensity when a buffer layer is present.

On a per-unit-area basis, replacement of 80% of the solar cell by the combination of the optimal POC and the optimal buffer layer will result in efficiency loss of just 14%. The use of very cheap dielectric materials for the POC and the buffer layer is very likely to offset this reduction.

IV. Concluding Remarks

Given that dielectric materials used in planar optical concentrators are cheaper than photovoltaic materials in common use,

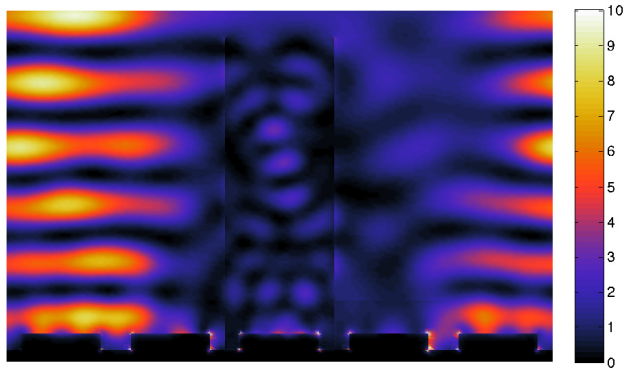

(a)

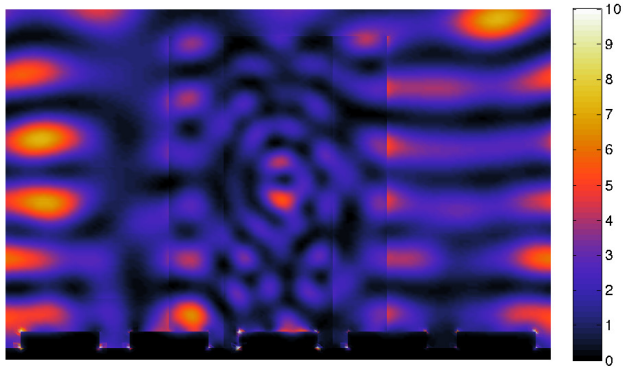

(b)

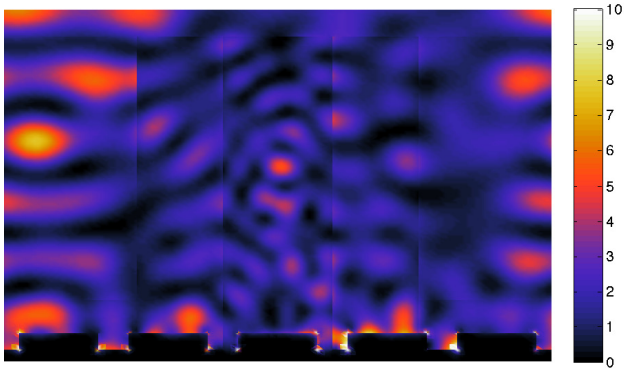

(c)

Fig. 12. Spatial distribution of $|\mathbf{E}(x, z, \lambda_0)|^2$ (V^2 m^{-2}) inside a unit cell of the light-harvesting structure the incident light is unpolarized, $\lambda_0 = 835.27$nm, the solar cell is made of GaAs, $N_d = 1$, and $n_b = 2.6$. (a) $2L_b = 0$, (b) $2L_b = 400$ nm, and (c) $2L_b = 630$ nm.

the incorporation of a POC can reduce the cost of fabricating solar-cell modules. Our previous work [2] had shown that a 4:1 POC made of a PMLID material could result in a loss of 54% (on a per-unit-area basis) in efficiency compared to a pure planar solar cell. Our current work improves upon that result through the insertion of a buffer layer between the PMLID material and the solar cell. Our calculations show that the buffer layer can have a wide tolerance in thickness from 150 to 350 nm, which is highly desirable from a manufacturing perspective, and may have a potential optimal thickness of 200 nm. More importantly, the addition of the buffer layer between the PMLID material and the solar cell improves the

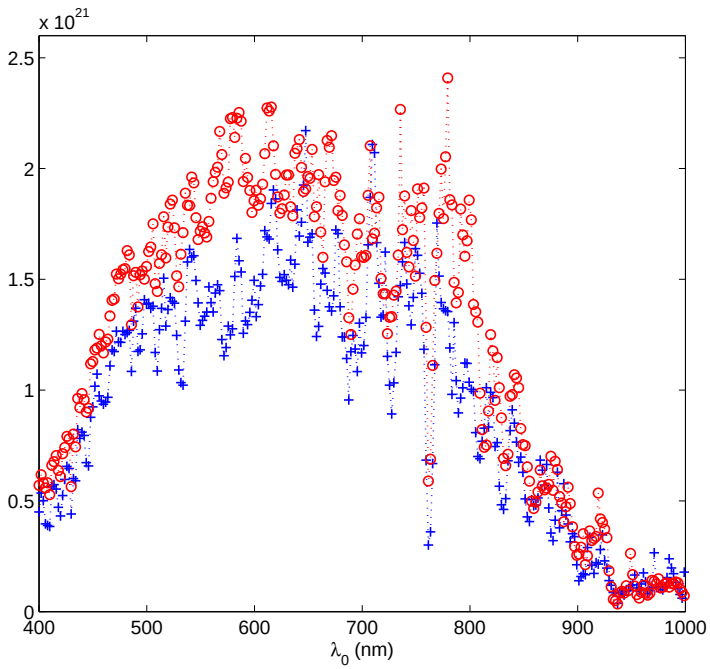

Fig. 13. Same as Fig. 7, except that $N_d = 3$.

spectrally averaged electron-hole pair density in a crystalline-silicon solar cell by 23% and in a GaAs solar cell by 31% compared to the same structure without the buffer layer for the same solar irradiance conditions.

Relative to a solar-cell module without the POC and the buffer layer, there is an efficiency loss of 40% for c-Si solar cells and 14% for GaAs solar cells accompanied by the combination of the optimal POC and the optimal buffer layer. These losses are amply compensated by the much lower costs of the dielectric materials in comparison to those of the semiconductors.

REFERENCES

[1] G. Kocher-Oberlehner, M. Bardosova, M. Pemble, and B. S. Richards, "Planar photonic solar concentrators for building-integrated photovoltaics," *Solar Energy Mater. Solar Cells*, vol. 104, no. 1, pp. 53–57, 2012.

[2] M. E. Solano, M. Faryad, P. B. Monk, T. E. Mallouk, and A. Lakhtakia. "Periodically multilayered planar optical concentrator for photovoltaic solar cells," *Appl. Phys. Lett.*, vol. 103, art. no. 191115, 2013.

[3] S. Bouchard and S. Thibault, "Graded-index planar waveguide solar concentrator," *Opt. Lett.*, vol. 39, no. 5, pp. 1197–1200, 2014.

[4] J. Yoon, A. J. Baca, S.-I. Park, P. Elvikis, J. B. Geddes III, L. Li, R. H. Kim, J. Xiao, S. Wang, T.-H. Kim, M. J. Motala, B. Y. Ahn, E. B. Duoss, J. A. Lewis, R. G. Nuzzo, P. M. Ferreira, Y. Huang, A. Rockett, and J. A. Rogers, "Ultrathin silicon solar microcells for semitransparent, mechanically flexible and microconcentrator module designs," *Nature Mater.*, vol. 7, no. 11, pp. 907–915, 2008.

[5] J. Yoon, L. Li, A. V. Semichaevsky, J. H. Ryu, H. T. Johnson, R. G. Nuzzo, and J. A. Rogers, "Flexible concentrator photovoltaics based on microscale silicon solar cells embedded in luminescent waveguides," *Nature Commun.*, vol. 2, art. no. 343, 2011.

[6] R. J. Knuesel and H. O. Jacobs, "Self-tiling monocrystalline silicon; a process to produce electrically connected domains of Si and microconcentrator solar cell modules on plastic supports," *Adv. Mater.*, vol. 23, no. 24, pp. 2727–2733, 2011.

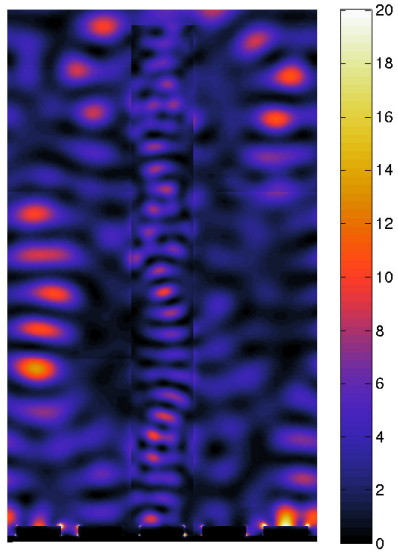

(a)

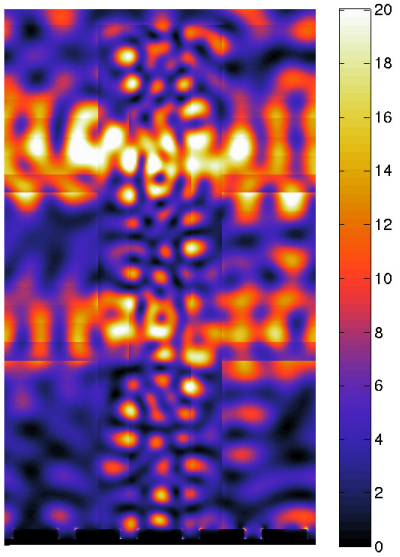

(b)

Fig. 14. Spatial distribution of $|\mathbf{E}(x,z,\lambda_0)|^2$ (V^2 m^{-2}) inside a unit cell of the light-harvesting structure the incident light is unpolarized, $\lambda_0 = 919.13$nm, the solar cell is made of c-Si, $N_d = 3$, and $n_b = 2.6$. (a) $2L_b = 0$ and (b) $2L_b = 400$ nm.

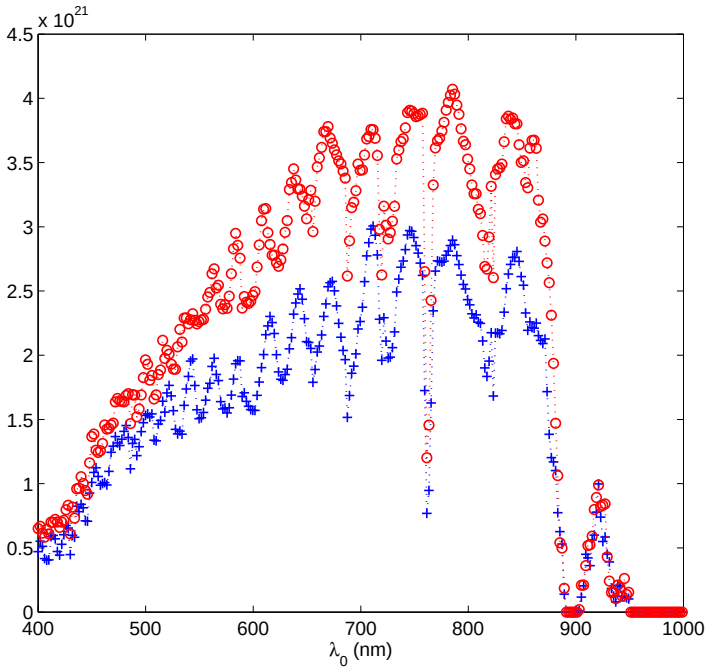

Fig. 15. Same as Fig. 11, except that $N_d = 3$.

[7] M. Faryad and A. Lakhtakia, "Enhancement of light absorption efficiency of amorphous-silicon thin-film tandem solar cell due to multiple surface-plasmon-polariton waves in the near-infrared spectral regime," *Opt. Eng.*, vol. 52, no. 8, art. no. 087106, 2013.

[8] M. Solano, M. Faryad, A. S. Hall, T. E. Mallouk, P. B. Monk, and A. Lakhtakia. "Optimization of the absorption efficiency of an amorphous-silicon thin-film tandem solar cell backed by a metallic surface-relief grating," *Appl. Opt.*, vol. 52, no. 5, pp. 966–979, 2013.

[9] P. B. Monk, *Finite Element Methods for Maxwell's Equations*. Oxford, United Kingdom: Oxford University Press, 2003.

[10] M. E. Solano, M. Faryad, A. Lakhtakia, and P. B. Monk, "Comparison of rigorous coupled-wave approach and finite element method for photovoltaic devices with periodically corrugated metallic backreflector," *J. Opt. Soc. Am. A*, vol. 31, no. xx, pp. xxxx–xxxx, 2014 (at press).

[11] http://www.cs.cmu.edu/\string~quake/triangle.html (accessed 15 July 2014).

[12] http://pveducation.org/pvcdrom/appendices/standard-solar-spectra (accessed 15 July 2014).

[13] http://refractiveindex.info/legacy/?group=CRYSTALS&material=Si (accessed 15 July 2014).

[14] http://refractiveindex.info/legacy/?group=CRYSTALS&material=GaAs&option=sopra (accessed 15 July 2014).

Manuel E. Solano received his B.S. degree in Mathematical Engineering from Universidad de Concepción, Concepción, Chile in 2007, and his Ph.D. degree in Scientific Computation in Mathematics from the University of Minnesota, Minneapolis, MN in 2011. He was a postdoctoral researcher in the Department of Mathematical Sciences at the University of Delaware, Newark, DE (2012–2013). He is currently an assistant professor in the Department of Mathematical Engineering at the Universidad de Concepción and a researcher at the Center for Research in Mathematical Engineering (CI^{2}MA) at the same institution. His research interests include numerical analysis and numerical methods applied to electromagnetism.

Greg D. Barber received his B.S. degrees in Physics (1991) and Ceramic Science and Engineering (1991) from the Pennsylvania State University, University Park, PA, USA. He then received his M.S. (1995) and Ph.D. (1998) degrees in Materials Science from the same institution. He is currently a Research Associate in the Penn State Institute for Energy and the Environment (PSIEE) after a post-doctoral appointment (1998–2000) and tenure as a Research Staff member (2000-2002) at the National Renewable Energy Laboratory (NREL) in Golden, CO. His

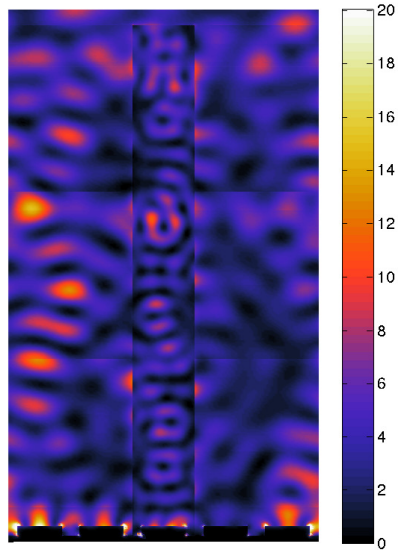

(a)

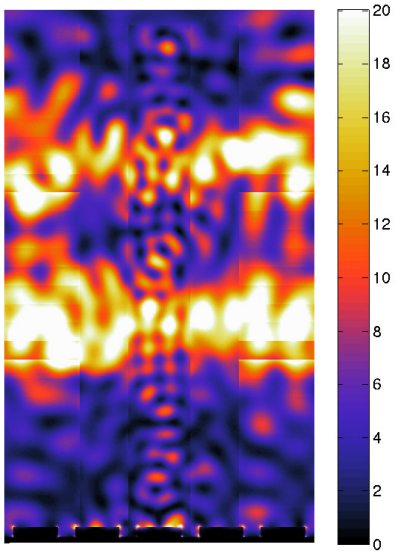

(b)

Fig. 16. Spatial distribution of $|\mathbf{E}(x,z,\lambda_0)|^2$ (V^2 m^{-2}) inside a unit cell of the light-harvesting structure the incident light is unpolarized, $\lambda_0 = 945.09$nm, the solar cell is made of GaAs, $N_d = 3$, and $n_b = 2.6$. (a) $2L_b = 0$ and (b) $2L_b = 630$ nm.

research focuses on solar radiation, thin film solar materials, carbon, and inorganic materials systems with particular emphasis on materials chemistry and scalable materials processing for solar energy production.

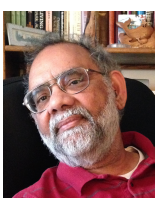

Akhlesh Lakhtakia received B.Tech. (1979) and D.Sc. (2007) degrees in Electronics Engineering from the Banaras Hindu University, Varanasi, India and the M.S. (1981) and Ph.D. (1983) degrees in Electrical Engineering from the University of Utah, Salt Lake City, UT. He is presently the Charles Godfrey Binder (Endowed) Professor of Engineering Science and Mechanics at the Pennsylvania State University, University Park, PA. He is a Fellow of SPIE, Optical Society of America, American Association for the Advancement of Science, American Physical Society, and Institute of Physics (UK). His current research interests include nanophotonics, surface multiplasmonics, complex materials including sculptured thin films and mimumes, thin-film solar cells, bone refacing, bioreplication, and forensic science.

Muhammad Faryad received his M.Sc. (2006) and M.Phil. (2008) degrees in Electronics from Quaid-i-Azam University, Islamabad, Pakistan, and his Ph.D. degree (2012) in Engineering Science and Mechanics from the Pennsylvania State University, University Park, PA. After serving two years as a postdoctoral research scholar in the same department at the Pennsylvania State University, he is now an Assistant Professor of Physics at Lahore University of Management Sciences, Lahore, Pakistan. His research interests include modeling of thin-film solar cells, electromagnetic surface waves, and sculptured thin films.

Peter B. Monk received his B.A. degree (1978) in Mathematics from Cambridge University, Sidney Sussex College, England, and his M.S. (1981) and Ph.D. (1982) degrees in Mathematics from Rutgers University, Piscataway, NJ. He is currently UNIDEL Professor in the Department of Mathematical Sciences at the University of Delaware, Newark, DE. His research focuses on numerical analysis and scientific computing, with particular emphasis on numerical methods in computational electromagnetism and inverse scattering.

Thomas E. Mallouk received an Sc.B. degree (1977) from Brown University, Providence, RI and a Ph.D. degree (1983) in Chemistry from the University of California, Berkeley, CA. After completing postdoctoral work at MIT in 1985, he joined the Chemistry faculty at the University of Texas at Austin. In 1993 he moved to the Pennsylvania State University, University Park, PA, where he is now Evan Pugh Professor with joint appointments in the Departments of Chemistry, Physics, and Biochemistry and Molecular Biology. His research focuses on the application of nanomaterials to problems in solar energy conversion, catalysis and electrocatalysis, motion on the nanoscale, and environmental remediation.